X-ray and NMR structure of human Bcl-xL, an inhibitor of programmed cell death

Yoon, Ho Sup; Sattler, Michael; Muchmore, Steven W.; Liang, Heng; Meadows, Robert P.; Harlan, John E.; Nettesheim, David G.; Chang, Brian S.; Thompson, Craig B.; Wong, Sui-Lam; Ng, Shi-Chung; Fesik, Stephen W.

1996

Muchmore, S. W., Sattler, M., Liang, H., Meadows, R. P., Harlan, J. E., Yoon, H. S., et al. (1996). X-ray and NMR structure of human Bcl-xL, an inhibitor of programmed cell death. Nature, 381, 335-341.

https://hdl.handle.net/10356/95496

https://doi.org/10.1038/381335a0

X-ray and NMR structure of human Bcl-x_L, an inhibitor of programmed cell death

Steven W. Muchmore*, Michael Sattlert † , Heng Liang † Robert P. Meadows‡, John E. Harlant †, Ho Sup Yoon †, David Nettesheim †, Brian S. Chang §, Craig B. Thompson§, Sui-Lam Wong‖¶, Shi-Chung Ng‖ & Stephen W. Fesikt †,

** Protein Crystallography, †NMR Research, ‡Research Computing and Information Sciences and ‖ Aging and Degenerative Diseases Research, Pharmaceutical Discovery Division, Abbott Laboratories, Abbott Park, Illinois 60064, USA*

§ Howard Hughes Medical Institute, and Departments of Medicine, Molecular Genetics and Cell Biology, The University of Chicago, Chicago, Illinois 60637, USA

¶Present address: Department of Biological Sciences, Division of Cellular, Molecular and Microbial Biology, University of Calgary, Calgary, Alberta T2N 1N4, Canada.

CORRESPONDENCE and requests for materials should be addressed to either S.W.M. (e-mail: muchmore@servo.pprd.abbott.com) or S.W.F. (e-mail: Fesik @steves.abbott.com).

Coordinates for the NMR and X-ray structures of Bc1-x_l have been deposited in the Brookhaven Protein Data Bank with accession numbers 1LXL and 1MAZ, respectively

The Bcl-2 family of proteins regulate programmed cell death by an unknown mechanism[1]. Here we describe the crystal and solution structures of a Bcl-2 family member, Bcl-x_L (ref. 2). The structures consist of two central, primarily hydrophobic α-helices, which are surrounded by amphipathic helices. A 60-residue loop connecting helices α 1 and α 2 was found to be flexible and non-essential for anti-apoptotic activity. The three functionally important Bcl-2 homology regions (BHl, BH2 and BH3)[3-5] are in close spatial proximity and form an elongated hydrophobic cleft that may represent the binding site for other Bcl-2 family members. The arrangement of the α-helices in Bcl-x_L is reminiscent of the membrane translocation domain of bacterial toxins, in particular diphtheria toxin and the colicins[6]. The structural similarity may provide a clue to the mechanism of action of the Bcl-2 family of proteins.

The structure of Bcl-x_L was determined by both X-ray crystallography and nuclear magnetic resonance (NMR) spectroscopy (Table 1). The structural studies were conducted on a biologically active form of human Bc1-x_L, lacking the putative transmembrane region at the carboxy terminus (Fig. 1 legend). Recombinant Bcl-x_L is monomeric, as determined by analytical ultracentrifugation, the lack of contact between molecules related by crystallographic two-fold axes in the unit cell, and the line widths observed in the NMR spectra (data not shown).

Using initial electron-density maps generated by multiple isomorphous replacement (MIR) and density-modification techniques, approximately 60% of the residues were modelled. Fitting the missing residues to the electron-density maps was guided by the secondary structure determined from NMR data and nuclear Overhauser enhancements (NOEs) observed between α-helices. Once a model was obtained from the combined structural information, the crystal and solution structures were determined separately using only the X-ray and NMR data, respectively. Although structures of $\mathrm{Bcl-x}_L$ could have been obtained independently by using either technique, the structure determination proceeded more rapidly by combining information from the two complementary methods. Both the X-ray and NMR structures are well defined (Table 1; Fig. l*a*, *b)* and agree well with each other (Fig. l*b*). The root-mean-square deviation (r.m.s.d.) for the α-carbon atoms (residues 6-18 and 85-195) between the crystal structure and averaged, energy-minimized NMR structure is 1.6 Å. The differences observed between the two structures for a region following the first helix (residues 19-27) and the loop between helices α5 and α6 (residues 156-160) appear to be due to crystal packing. Residues 101-103 differ in the X-ray and NMR structures, but these residues are part of a flexible hydrophilic loop, and are poorly defined by both techniques.

The structure of Bc1-x_L, consists of two central α -helices (α5 and α6), which are about 30 Å in length, flanked on one side by α3 and α4 and on the other by αl, α1 and α7 (Fig. l*c*). The two central helices contain predominantly hydrophobic residues, and are arranged in an antiparallel fashion, with a crossing angle of 23°. Helix α6 contains a kink at Pro 180 that causes a change in the direction of this helix. The C-terminal helix (α7) is connected to α6 by an irregular turn composed of two glycines (Gly 186 and Gly 187), which are largely conserved. In Bcl-x_L, Gly 187 adopts (ϕ/ψ angles not normally observed for other residue types. This could explain its conservation (Fig. 1d) and the loss of binding to Bax on mutation of Gly 187 in Bc1-x_L, (ref. 7). The N-terminal helix forms extensive hydrophobic interactions with α2, α5 and α6, and seems to be important for stabilizing the structure of the protein. This is consistent with the observation that deletion mutants in this region of Bcl-2 fail to protect against cell death induced by growth-factor withdrawal or to suppress Bax-mediated cytotoxicity[8,9].

No electron density was observed for residues Ser 28 to Val 80. In addition, no medium- or long-range NOEs were detected for the residues in this region, and the chemical shifts and vicinal coupling constants $^3(J_{NH,H\alpha})$ are consistent with those in a random coil. To obtain a direct measure of protein flexibility, two-dimensional ^{15}N-^{1}H heteronuclear NOE experiments were conducted on uniformly ^{15}N-labelled Bc1-x_L, (Fig. 2a). The negative NOE values observed for residues 35-78 (Fig. 2a, *b)* indicate that this region is highly mobile in solution relative to the overall tumbling rate of the molecule. This flexible loop corresponds to a region of low sequence

homology and variable length among Bc1-2 family members (Fig. 1d). To determine whether this region is required for the anti-apoptotic properties of Bcl-x_L, a mutant in which amino acids 26-83 were deleted and replaced by four alanines (HA-Bc1-x_L Δ26-83) was cloned into an expression vector and stable transfectants were analysed for their ability to survive interleukin-3 (IL)-3 withdrawal in comparison to cells transfected with the wild-type gene (HA-Bcl-x_L,). The survival of cells transfected with the deletion mutant was at least as good as the survival of cells stably transfected with full-length Bc1- x_L (Fig. 2c). Deletions of smaller numbers of amino acids in Bcl-x_L, (Δ26-63 and Δ46-83) also retained anti-apoptotic properties (data not shown). These data suggest that Bcl-x_L lacking the large flexible loop still retains the anti-apoptotic function when overexpressed.

Bcl-2 proteins share homology domains BH1 and BH2 (Fig. 1*d*), and mutations within these regions in Bcl-2 or Bcl-x_L, abrogate the anti-apoptotic activity and block the heterodimerization with other members of the Bcl-2 family (for example, Bax or Bak) that promote programmed cell death[3,10,11]. A third region of homology among Bcl-2 proteins (BH3) has been recognized and found to be essential for the activity of the death-promoting proteins[4,5]. These functionally important regions (BH1, BH2 and BH3) are in close spatial proximity (Fig. 1*c*), and form an elongated hydrophobic cleft in Bcl-x_L (Fig. *3a, b*). This cleft may be the site of interaction with death-promoting proteins such as Bax and Bak. Indeed, mutations of a highly conserved glycine (Gly 138), which forms part of this groove (Fig. 3*b*, red), inhibit the death-repressor activity of Bel-2 and Bc1-x_L, and block binding to Bax[3]. Although this glycine was proposed to play an important structural role[3], its ϕ and ψ angles (-56° and 41°, respectively) are within the range of other amino acids. Thus Gly 138 seems to be important because amino acids with bulkier side chains could potentially block access to this pocket. Further evidence to support the functional importance of this region is the high conservation of the hydrophobic residues (Fig. 1*d*) that line this cleft which are solvent exposed (Fig. 3*a*, *b).*

The sequence homology between Bcl-x, and other members of the Bcl-2 family (Fig. 1*d*) suggests that these proteins exhibit a similar fold. Bcl-x_L, resembles the membrane insertion domain found in bacterial toxins[6], in particular the diphtheria toxin and the colicins. Like Bcl-x_L, these membrane insertion domains contain two central helices consisting of apolar residues, and are long enough to span a membrane. Helices α5 and α 6 and three of the surrounding amphipathic helices (al, α3 and α4) in the Bcl-x_L structure align well (r.m.s.d., 2.0 Å for 50 Cα positions) with corresponding elements of the transmembrane domain of diphtheria toxin (Fig. 3*c*).

The diphtheria-toxin translocation domain is thought to dimerize and form a pH-dependent membrane pore[12]. By analogy, Bc1-2 proteins may form pores in the

cytoplasmic membranes where they localize. The insertion of Bc1-2 proteins like the bacterial proteins, may be regulated by signals dependent on voltage and pH. Membrane insertion and pore formation might promote cell death by dissipating the essential electrochemical gradients necessary for cellular homeostasis, or alternatively could inhibit cell death by eliminating a chemical imbalance and restoring cellular homeostasis. Bcl-2 overexpression stabilizes calcium homeostasis between the cytoplasm and the ER[13].Bcl-2 has also been shown to prevent mitochondria] permeability transition, which results in the uncoupling of electron transport[14]. These data suggest that Bc1-2 proteins may directly or indirectly affect the permeability of these important cytoplasmic organelles and thus regulate cellular homeostasis and apoptosis.

ACKNOWLEDGEMENTS.

We thank T. Holzman, J. Severin, K. Walter and H. Zhang for help in protein preparation; S. Snyder for analytical ultracentrifugation studies; and S.W.M. thanks C. AbadZapatero, C. Park and V. Giranda for discussions.

REFERENCES

[1] Korsmeyer, S. J. Trends Genet. **11**, 101-105 (1995).

[2] Boise, L. H. *et al. Cell* **74,** 597-608 (1993)

[3] Yin, X.-M., Oltvai, Z. N. & Korsmeyer, S. J. *Nature* **369,** 321-323 (1994).

[4] Chittenden, T. et *al. EMBO J.* **14,** 5589-5596 (1995).

[5] Boyd, J. M. et *al. Oncogene* **11,** 1921-1928 (1995).

[6] Parker, M. W. & Pattus, F. *Trends biochem. Sci.* **18,** 391-395 (1993).

[7] Cheng, E. H.-Y., Levine, B., Boise, L. H., Thompson, C. B. & Hardwick, J. M. *Nature* **379,** 554-557 (1996).

[8] Borner, C. *J. Cell Biol.* **126,** 1059-1068 (1994).

[9] Hanada, M., Aime-Sempe, C., Sato, T. & Reed, J. C. *J. biol. Chem.* **270,** 11962-11969 (1995).

[10] Sedlak, T. W. *et al. Proc. natn. Acad. of Sci. U.S.A.* **92,** 7834-7838 (1995).

[11] Yang, E. *et al. Cell* **80,** 285-291 (1995).

[12] London, E. *Biochim. biophys. Acta* **1113,** 25-51 (1992).

[13] Lam, M. *et al. Proc. natn. Acad. Sci. U.S.A.* **91,** 6569-6573 (1994).

[14] Zamzami, *et al. J. exp. Med.* **182,** 367-377 (1995).

[15] Carson, M. J. J. *Molec. Graph.* **5,** 103-106 (1987).

[16] Fang, W., Rivard, J. J., Mueller, D. L. & Behrens, T. W. *J. lmmunol.* **153,** 4388-4398 (1994).

[17] Otwinowski, Z. *Proceedings* of *the CCP4 Study Weekend: Isomorphous Replacement and Anomalous Scattering* (eds Wolf, W., Evans, P. R. & Leslie, A. G. W.) 80-86 (SERC Daresbury Laboratory, Warrington, UK, 1991).

[18] *CCP4: A Suite of Programs for Protein Crystallography* (SERC Daresbury Laboratory, Warrington, UK, 1979)

[19] Jones, T. A., Zou, J.-Y., Cowan, S. W. & Kjelgaard, M. *Acta crystallogr. A* **47,** 110 (1991).

[20] Reed, R. J. *Acta crystallogr. A* **42,** 140-149 (1986).

[21] Brünger, A. T. *X-PLOR* 3.1 (Yale University, New Haven, CT, 1992).

[22] Yamazaki, T., Lee, W., Arrowsmith, S. H., Muhandiram, D. R. & Kay, L. E. *J. Am. chem. Soc.* **116,** 11655-11666 (1994).

[23] Clore, G. M. & Gronenborn, A. M. *Meth. Enzym.* **239,** 349-363 (1994).

[24] Logan, T. M., Olejniczak, E. T., Xu, R. X. & Fesik, S. W. *FEES Lett.* **314,** 413-418 (1992).

[25] Neri, D., Szperski, T., Otting, G., Senn, H. & Wüthrich, K. *Biochemistry* **28,** 7510-7516 (1989).

[26] Vuister, G. W., Kim, S.-J., Wu, C. & Bax, A. J. *Am. chem. Soc.* **116,** 9206-9210 (1994).

[27] Kuboniwa, H., Grzesiek, S., Delaglio, F. & Bax, A. *J. Biomolec. NMR* **4,** 871-878 (1994).

[28] Kuszewski, J., Nilges, M. & Brünger, A. T. *J. Biomolec. NMR* **2,** 33-56 (1992).

[29] Farrow, N. A. *et al. Biochemistry* **33,** 5984-6003 (1994).

[30] Choe, S. et *al. Nature* **357,** 216-222 (1992).

List of Figures

Figure 1 a,Electron density from the final A 2.2Å $2F_o$- F_c map. Blue map contours are 1 r.m.s.d. from the mean of the map. The Bcl-x_L model is shown in the stick representation, in white (C atoms), blue (N atoms) and red (0 atoms). The region shown is the hydrophobic cleft near the BH1 domain. *b,* Stereo view of the backbone (N, Cα, C') of 20 superimposed NMR-derived structures of BcI-x_L ,(residues 3-26, 85-196) (black) on an N-Cα-C' trace of the same residues in the X-ray structure (red). c, Ribbons[15] depiction of the averaged, minimized NMR of BH1, BH2 and BH3 regions are yellow, red and green, respectively. *d,* Sequence alignment of Bcl-2 family members. The sequence of human Bcl-x_L is shown along with those of human Bcl-2, Bak, Bax Mcl-1 and *Caenorhabditis elegans* CED-9. Dark blue and green boxes designate residues that are identical or similar (as measured by hydrophobicity) to Bcl-x_L, respectively. The helices in the X-ray and NMR structures are indicated. The numbers above the sequences correspond to Bcl-x_L,

METHODS. Protein expression and purification: Human BcI-x_L[2] (residues 1-209) lacking the C-terminal hydrophobic region was expressed in *Escherichia* coli using the pET29b vector (Novagen). The recombinant protein contained four extra amino acids (MSMA-) at the N terminus, owing to cloning artefacts, and a polyhistidine tag (-LEHHHHHH) at the C terminus to facilitate purification. To confirm that the Bcl-x_L protein analysed by both X-ray crystallography and NMR spectroscopy had biological activity, the coding region of the construct was introduced into an IL-3-dependent cell line, and transfectants survival was compared to cells transfected with wild-type BcI-x_L,, or a control plasmid. For a period of 24 h after IL-3 withdrawal, the viability of control cells was 28.4 ± 0.7%; transfected cells containing the construct displayed a viability of 85.0 + 0.4%, (comparable to previous[16] C-terminal truncations of Bcl-x_L; and cells transfected with wild-type Bcl-x_L had a viability of 97.1 ± 0.1%. These data suggest that the protein retains the ability of Bcl-x_L to function as an antiapoptotic gene. For crystallization, cells of *E.* colI strain BL21(DE3) transformed with the expression vector were grown at 37 °C on LB medium. For NMR experiments, uniformly ^{15}N- or ^{15}N-,^{13}C-labelled protein was prepared by growing the *E.* coli strain HMS174(DE3) overexpressing Bcl-x_L on M9 medium containing $^{15}NH_4CI$ with or without [U-^{13}C]-glucose. A uniformly ^{15}N-,^{13}C-labelled and fractionally deuterated protein sample was also prepared by growing cells with 75% $^2H_20$. Recombinant BcI-x_L was purified by affinity chromatography on a nickel-IDA column (Invitrogen). Further purification was achieved by reversed-phase chromatography of the denatured protein on a C4 or C8 column, followed by refolding through the gradual removal of the denaturant by dialysis. X-ray crystallography: Crystals of Bcl-x_L, were obtained by screening limited factorial crystallization solutions (Hampton Research). Crystals suitable for diffraction analysis were obtained by hanging-drop vapour diffusion. Protein was

concentrated to 25 mg $m1^{-1}$ in 50 mM Tris, pH 7.4, and equilibrated against 28-31% (w/v) PEG 4,000, 0.2 M ammonium acetate, 0.1 M sodium citrate, pH 7.5. The crystals are tetragonal, space group $P4_12_12$, a = b = 63.5 Å, c = 110.5, $\alpha = \beta = \gamma$ = 90.0°, and contain one copy of the Bc1-x_L protein per asymmetric unit. Diffraction data were collected at 110 K using Cu-Kα radiation, on an R-Axis IIc area detector (Molecular Structure Corporation). Intensity data were evaluated using the HKL[17] suite of programs. Heavy-atom difference Patterson maps were interpreted by inspection to derive the heavy-atom substituent positions. These positions were refined using MLPHARE[18], and phase refinement by real-space density modification was computed using DM[18]. Initial model-building studies used 2.7Å resolution electron-density maps, interpreted with the graphics program 0[19]. Partial models were used to calculate phases that were then combined with the MIR phase set using SIGMAA[29] to produce improved electron-density maps. After models that agreed well with both the NMR and X-ray data were available, a final phase refinement experiment was calculated using a mask derived from the consensus structure. The final phase refinement extended to 2.2 Å resolution, and maps derived from these experiments were used to build a model used in computational refinement using X-PLOR[21]. NMR spectroscopy: NMR samples contained 1-3 nM Bcl-x_L in 20 mM sodium phosphate (pH 7.3), 5 mM perdeuterated DTT, 1mM perdeuterated EDTA, $H_20/^2H_20$ (9/1) or $^2H_20$. NMR spectra were acquired at 30 °C on a Bruker DMX500 or AMX600 NMR spectrometer. The ^1H, ^{13}C and ^{15}N resonances of the backbone were assigned from a series of deuterium-decoupled triple-resonance experiments (HNCA, HN(C0)CA, HN(CA)CB and HN(COCA)CB)[22] recorded using the uniformly ^{15}N-,^{13}C labelled and fractionally deuterated protein. The side-chain signals were assigned from three-dimensional (3D) HCCH total correlation spectroscopy (TOCSY)[23] and HBHA(CO)NH[23] experiments on [U-^{15}N-,^{13}Q-labelled samples and from HC(CO)NH-TOCSY[24] experiments on the [U-15N– 13C]-labelled and fractionally deuterated sample. Stereospecific assignment of methyl groups of Val and Leu residues were obtained using a fractionally ^{13}C-labelled sample[25]. Distance restraints were obtained from ^{15}N- or ^{13}C-resolved 3D NOESY experiments[23] and a ^{13}C-separated, ^{13}C-filtered 3D NOESY acquired on a ^{12}C-Phe, [U-^{15}N,^{13}C] sample[26]. The ϕ angle restraints were based on the $^3J_{HNH\alpha}$ coupling constants measured in a HNHA experiment[27]. Slow-exchanging amide protons were identified from a series of $^1H/^{15}N$ HSQC spectra recorded after $^2H_20$ was added to a lyophilized ^{15}N-labelled Bcl-x_L sample. Structures of Bc1-x_L were calculated with a distance geometry/simulated annealing protocol[28] using X-PLOR[21]. Structure calculations used 2,086 proton/proton distance restraints, 108 hydrogen-bond distance restraints derived for 54 slow-exchanging amide protons, and 60 ϕ angle restraints. NOE-derived restraints were categorized as strong (1.8-3 Å), medium (1.8-4 Å), or weak (1.8-5Å) based on the observed NOE intensities.

Figure2 a, Steady-state heteronuclear $^{15}N\{^{1}H\}$-NOE for the backbone amides of Bcl-x_L. *b,* Ribbon depiction of the energy-minimized average NMR structure. Residues exhibiting negative ^{15}N $\{^{1}H\}$-NOE values are blue. This schematic drawing illustrates the size of the unstructured loop relative to the rest of the protein. The conformation of the loop shown is one of many that satisfy the NMR-derived restraints. c, Functional analysis of Bc1-x_L Δ26-83 mutants. Top right, Haemagglutin (HA)-tagged Bcl-x_L Δ26-83 (diamonds) mutant protects at least as well as the HA-Bc1-x_L (circles) against IL-3 withdrawal-induced cell death. Control transfected cells (squares) die rapidly following IL-3 withdrawal. Bottom right, western blot analysis indicating the presence of Bcl-x_L proteins in transfected cells. Arrows indicate the expected sizes of the HA-Bc1-x_L Δ26-83 (lower) or the HA-Bcl-x_L wild-type protein (upper).

METHODS. Heteronuclear $^{15}N\{^{1}1\text{-}1\}$-NOE was measured using a pulse sequence that incorporates water flip-back, gradient coherence selection, and sensitivity-enhancement schemes[29]. Two data sets, each consisting of spectra with proton saturation (NOE spectrum) and without proton saturation NONOE spectrum), were collected. The $^{15}N\{^{1}1\}$-NOE was calculated as the ratio of the heights of corresponding peaks in the NOE and NONOE spectra. Values from two data sets were averaged, error bars represent the deviation of individual values. After the NMR measurements, SDS—PAGE verified that the Bc1-x_L polypeptide was not proteolyzed. A deletion mutant of Bcl-x_L in which amino acids 26-83 have been replaced by four alanines was introduced into the pSSFV-neo expression plasmid. A HA tag was engineered on the 5' end to allow for the detection of the protein product in stable transfectants. This construct was stably introduced in FL5.12 cells by electroporation as previously described[2], and the survival properties of cells expressing the HA-Bc1-x_L Δ 26-83 protein were compared with survival properties of cells transfected with either HA-tagged Bcl-x_L wild type or a neomycin control plasmid. At time zero, transfectants were removed from IL-3-containing media and resuspended in 2.0 ml of media lacking IL-3. Survival was then followed at daily intervals by analysing the cells for propidium iodide exclusion by flow cytometry. Each sample was analysed in triplicate; mean and s.d. are shown. The expression of NA-BcI-x_L Δ26-83 and HA-Bc1-x_L, was confirmed by western blot analysis.

Figure3 a, Ribbons stereo view of the X-ray structure of Bcl-x_L showing the position of hydrophobic side chains (yellow) and Gly-138 (red) in the region of the proposed binding site. *b,* Stereo view of a surface representation of BcI-x_L in the same orientation as a. Ile, Leu, Val, Phe, Trp, Tyr and Ala are shown in yellow, and Gly 138 in red. c, Structural comparison of Bc1-x_L (left) and the transmembrane domain of diphtheria toxin[30] (right). The two central helices

are shown in red, and the amphipathic α-helices common to both proteins are blue or yellow.

List of Table

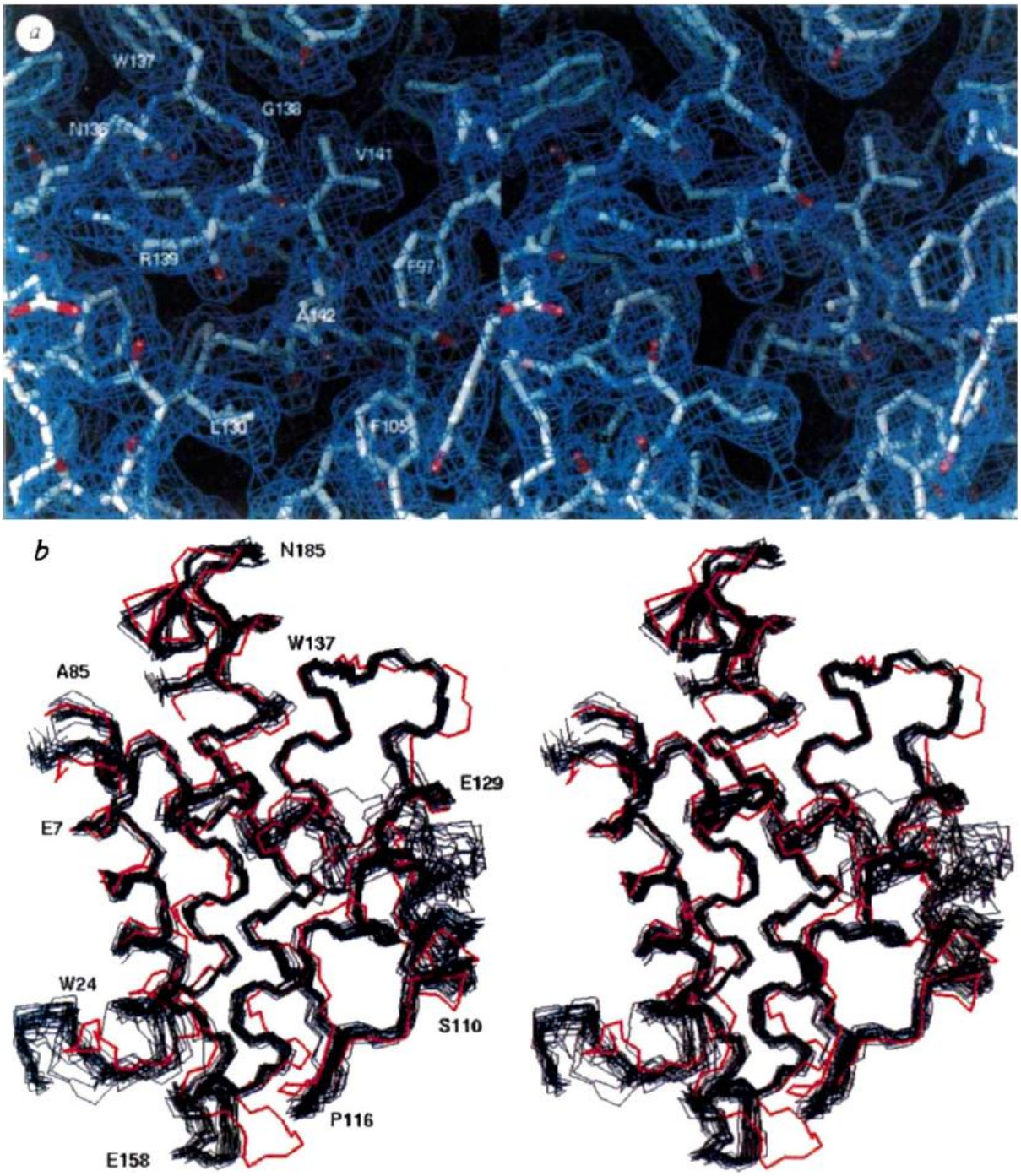
a
W137
G138
V141
R139
F97
A142
L130
F105
b
N185
W137
A85
E129
E7
W24
S110
P116
E158

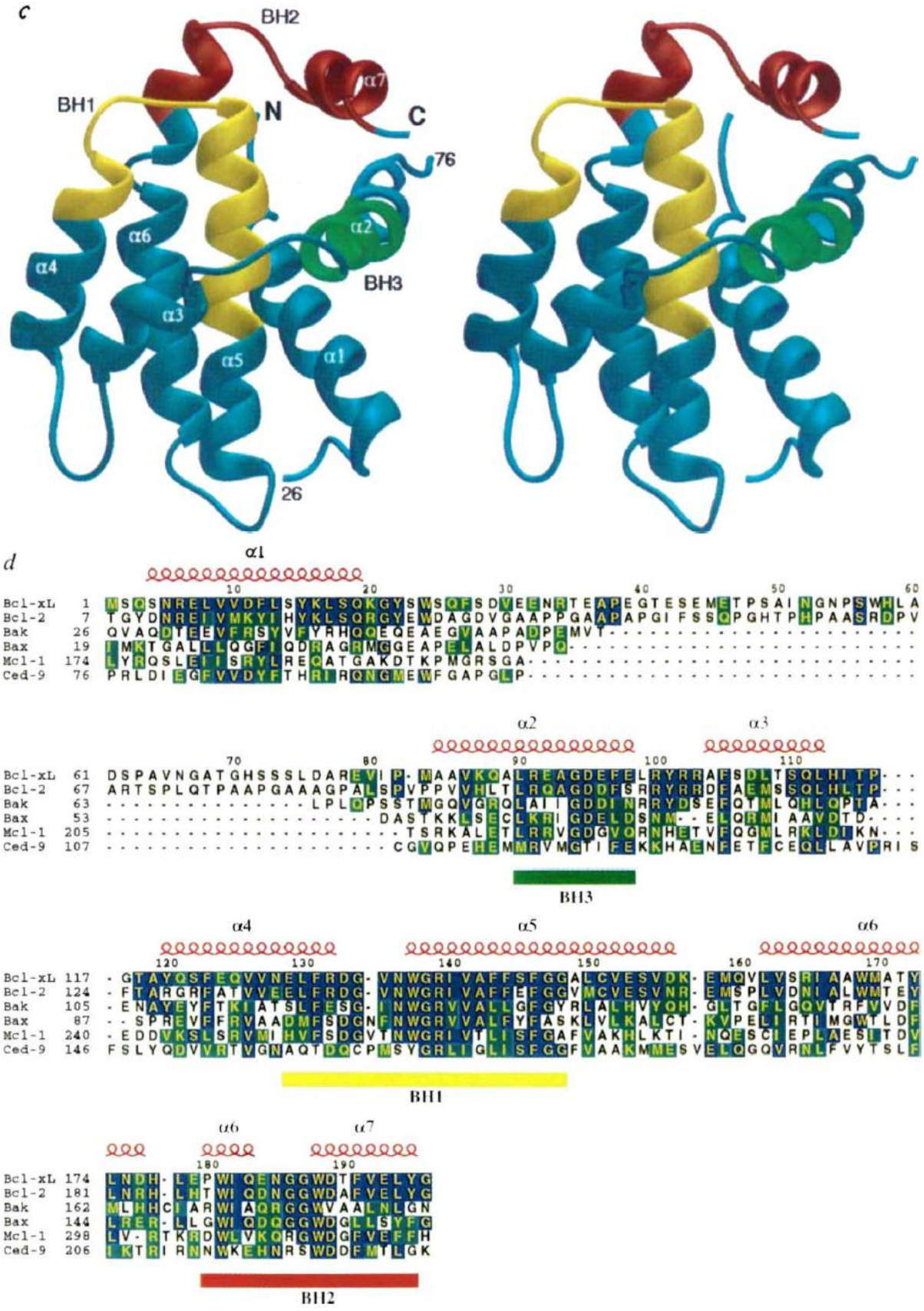
c
BH2
α7
BH1
N
C
76
α6
α2
α4
BH3
α3
α5
α1
26
d
α1
Bcl-xL 1 MSQSNRELVVDFLSYKLSQKGYSWSQFSDVEENRTEAPEGTESEMETPSAINGNPSWHLA
Bcl-2 7 TGYDNREIVMKYIHYKLSQRGYEWDAGDVGAAPPGAAPAPGIFSSQPGHTPHPAASRDPV
Bak 26 QVAQDTEEVFRSYVFYRHQQEQEAEGVAAPADPEMVT
Bax 19 IMKTGALLLQGFIQDRAGRMGGEAPELALDPVPQ
Mcl-1 174 LYRQSLEIISRYLREQATGAKDTKPMGRSGA
Ced-9 76 PRLDIEGFVVDYFTHRIRQNGMEWFGAPGLP
α2
α3
Bcl-xL 61 DSPAVNGATGHSSSLDAREVIP-MAAVKQALREAGDEFELRYRRAFSDLTSQLHITP
Bcl-2 67 ARTSPLQTPAAPGAAAGPALSPVPPVVHLTLRQAGDDFSRRYRRDFAEMSSQLHLTP
Bak 63 LPLQPSSTMGQVGRQLAIIGDDINRRYDSEFQTMLQHLQPTA
Bax 53 DASTKKLSECLKRIGDELDSNM-ELQRMIAAVDTD
Mcl-1 205 TSRKALETLRRVGDGVQRNHETVFQGMLRKLDIKN
Ced-9 107 CGVQPEHEMMRVMGTIFEKKHAENFETFCEQLLAVPRIS
BH3
α4
α5
α6
Bcl-xL 117 GTAYQSFEQVVNELFRDG-VNWGRIVAFFSFGGALCVESVDK-EMQVLVSRIAAWMATY
Bcl-2 124 FTARGRFATVVEELFRDG-VNWGRIVAFFEFGGVMCVESVNR-EMSPLVDNIALWMTEY
Bak 105 ENAYEYFTKIATSLFESG-INWGRVVALLGFGYRLALHVYQH-GLTGFLGQVTRFVVDF
Bax 87 SPREVFFRVAADMFSDGNFNWGRVVALFYFASKLVLKALCT-KVPELIRTIMGWTLDF
Mcl-1 240 EDDVKSLSRVMIHVFSDGVTNWGRIVTLISFGAFVAKHLKTI-NQESCIEPLAESITDV
Ced-9 146 FSLYQDVVRTVGNAQTDQCPHSYGRLIGLISFGGFVAAKMMESVELQGQVRNLFVYTSLF
BH1
α6
α7
Bcl-xL 174 LNDH-LEPWIQENGGWDTFVELYG
Bcl-2 181 LNRH-LHTWIQDNGGWDAFVELYG
Bak 162 MLHHCIARWIAQRGGWVAALNLGN
Bax 144 LRER-LLGWIQDQGGWDGLLSYFG
Mcl-1 298 LV-RTKRDWLVKQRGWDGFVEFFH
Ced-9 206 IKTRIRNNWKEHNRSWDDFMTLGK
BH2

Figure 1

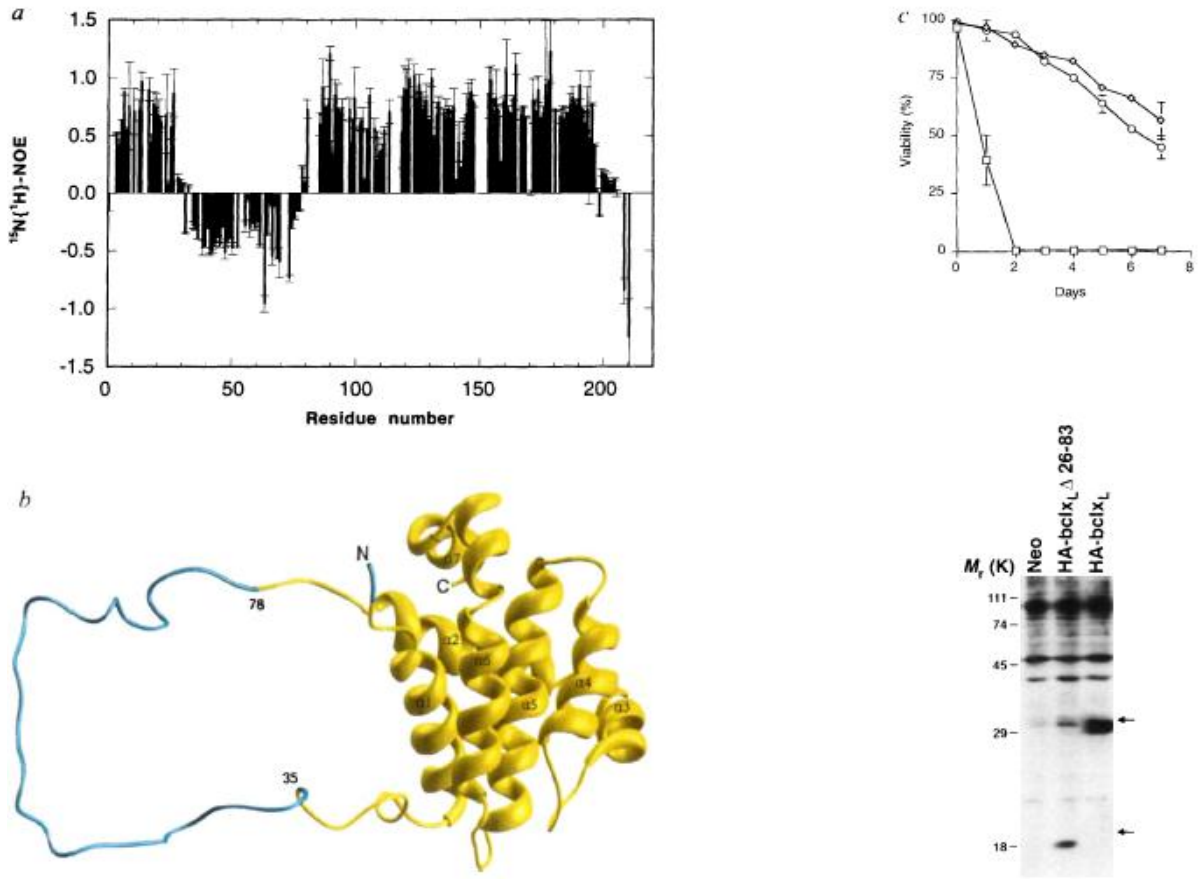
a
1.5
1.0
0.5
0.0
-0.5
-1.0
-1.5
$^{15}N\{^1H\}$-NOE
0
50
100
150
200
Residue number
b
N
C
78
35
α2
α5
α4
α1
α3
c
100
75
50
25
0
Viability (%)
0
2
4
6
8
Days
M_r (K)
Neo
HA-bclx$_L$Δ 26-83
HA-bclx$_L$
111
74
45
29
18

Figure 2

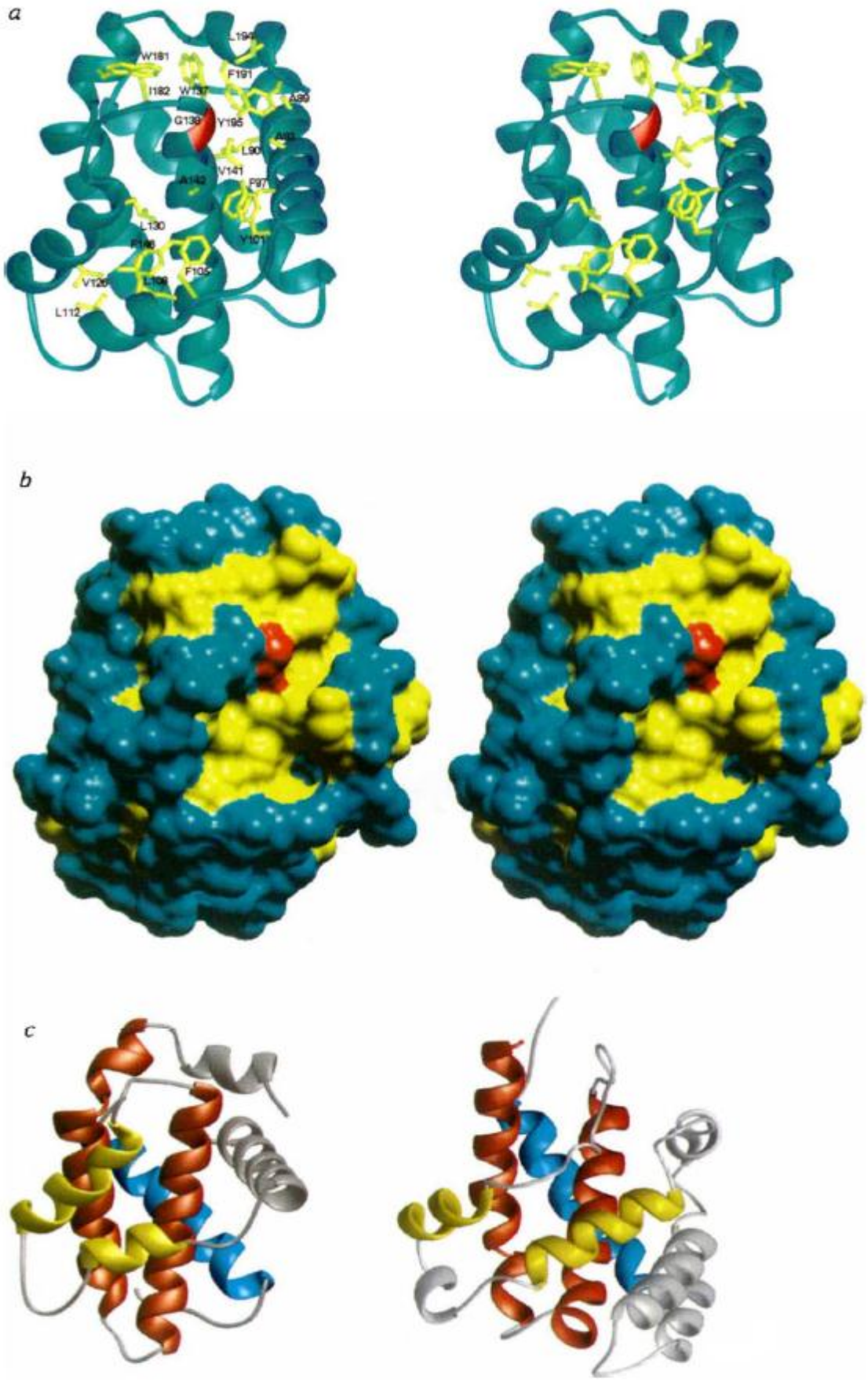
a
W181
F191
I182
G139
Y195
L90
V141
A143
P97
L130
V126
L112
F105
b
c

Figure 3

(*a*) X-ray diffraction data statistics

Crystal*	Resolution (Å)	Unique reflections†	R_{merge} (%)‡	R_{iso} (%)§	Number of sites	Phasing power‖
Native	2.2	11,139 (94, 80)	5.5, 22.2			
EMTS	2.6	7,233 (97, 95)	5.6, 16.1	16.6, 19.7	1	1.42, 0.93
PIP	3.5	7,004 (99, 98)	3.3, 7.4	16.2, 16.7	3	0.92, 0.61
K_2PtCl_4	2.7	6,638 (92, 94)	5.6, 19.7	16.1, 12.3	2	1.51, 1.33
TMLA	2.7	7,250 (97, 94)	5.2, 18.4	26.5, 20.9	3	1.38, 1.15

(*b*) Structural statistics of refined X-ray model

Total reflections (7–2.2 Å)	Working set:	9,995	Test set:	1,144
Number of non-H atoms	Protein:	1,145	Solvent:	154
R-factors	Standard:	19.2	Free:	25.9
Average *B*-factors (Å^2)	Main chain:	16.8	Side chain:	22.3
Stereochemical deviations	Bond lengths:	0.014	Bond angles:	1.92°

(c) Structural statistics of NMR models

R.m.s.d. from experimental distance restraints (Å)¶

	⟨SA⟩	$\langle\overline{SA}\rangle_r$
Intra-residue (607)	0.007 ± 0.002	0.008
Sequential (598)	0.012 ± 0.004	0.017
Medium-range (379)	0.018 ± 0.003	0.014
Long-range (502)	0.010 ± 0.002	0.009
Hydrogen bonds (108)	0.030 ± 0.004	0.024

R.m.s.d. from experimental torsional angle restraints (deg)#

Φ angles (60)	0.23 ± 0.09	0.11

X-PLOR potential energies (kcal mol^{-1})

	⟨SA⟩	$\langle\overline{SA}\rangle_r$		⟨SA⟩	$\langle\overline{SA}\rangle_r$
E_{tot}	219 ± 12	271	E_{bond}	17 ± 1	22
E_{ang}	133 ± 5	164	E_{imp}	20 ± 1	20
E_{repel}	27 ± 4	45	E_{noe}	20 ± 3	19
E_{cdih}	0.2 ± 0.1	0.05	$E_{L\text{-}J}$☆	−1,023 ± 16	−952

Cartesian coordinate r.m.s.d. (Å)

⟨SA⟩ versus $\langle\overline{SA}\rangle$	N, Cα and C′	all heavy atoms
Residues 6–18, 85–195	0.61 ± 0.12	1.26 ± 0.15
Residues 6–18, 85–100, 104–195	0.54 ± 0.10	1.03 ± 0.12

⟨SA⟩ is the ensemble of 20 simulated-annealing structures; $\langle\overline{SA}\rangle$ is the mean atomic structure obtained by averaging the coordinates of the individual ⟨SA⟩ following a least-squares superposition of the backbone heavy atoms (N, Cα, C′) for residues 6–18 and 85–195; $\langle\overline{SA}\rangle_r$ is the energy-minimized, averaged structure. The X-PLOR F_{repel} function was used to simulate can der Waals interactions with a force constant of 4.0 kcal mol^{-1} Å^{-4} with atomic radii set to 0.8 times their CHARMM values.

* Bcl-x_L crystals were derivatized by soaking crystals in stabilization solution (22% PEG 4,000, 200 mM ammonium chloride, 50 mM Tris, pH 7.5) in which the following compounds had been dissolved: EMTS, 3 mM sodium ethylmercurithiosalicylate, 24 h; PIP, 4 mM di-μ-iodobis(ethylenediamine) diplatinum (II) nitrate, 48 h; K_2PtCl_4, 5 mM potasium tetrachloroplatinate (ii), 24 h; TMLA, 10 mM trimethyl lead acetate, 7 days.

† The total number of merged reflections; the two numbers following the total are the overall percentage observed, and the percentage observed in the last reflection shell (~0.1 Å width).

‡ $R_{merge} = \Sigma_h\Sigma_i|I_{hi} - \langle I_{hi}\rangle|/\Sigma_h\Sigma_i|I_{hi}|$, where *h* specifies unique reflection indices, and *i* indicates symmetry equivalent observations of *h* and $\langle I_h\rangle$ is the mean value. The first number is the value for all data, and the second refers to the highest resolution shell.

§ $R_{iso} = \Sigma_h||F_{ph}| - |F_p||/\Sigma_h|F_p|$, where $|F_{ph}|$ and $|F_p|$ are the measured structure factor amplitudes of the derivative and native structures. The two percentages refer to the overall and last resolution shell, respectively.

‖ Phasing power is the ratio of the calculated heavy-atom structure factor amplitude to the closure error in the phasing model, and the two numbers are the overall value, and the value in the last resolution shell, respectively.

¶ NOE-derived distance restraints were used with a square-well potential (F_{noe} = 50 kcal mol^{-1} Å^{-2}). In addition, hydrogen bonds were included and given bounds of 1.8–2.4 Å (H–O) and 2.8–3.2 Å (N–O). No distance restraint was violated by more than 0.4 Å in any of the final structures. Medium-range NOEs correspond to those observed between protons separated by more than one and less than five residues in the primary sequence, and long-range NOEs are between protons separated by five or more residues.

Torsional Φ angle restraints were applied with values of −60 ± 40° for $^3J_{HNH\alpha}$ coupling constants smaller than 5.8 Hz. These were applied only in α-helical regions. Force constants of 200 kcal mol^{-1} rad^{-2} were applied for all torsional restraints. No torsional angle restraint was violated by more than 3° in any of the final structures.

☆ The Lennard-Jones potential was not used during any refinement stage.

Table 1